

Anisotropic magnetic properties of light rare-earth diantimonides

S. L. Bud'ko and P. C. Canfield

Ames Laboratory and Department of Physics and Astronomy, Iowa State University, Ames, Iowa 50011

C. H. Mielke and A. H. Lacerda

National High Magnetic Field Laboratory, Los Alamos Facility, Los Alamos National Laboratory, Los Alamos, New Mexico 87545

(Received 2 June 1997; revised manuscript received 13 February 1998)

Results are presented of anisotropic temperature and field-dependent magnetization $M(H, T)$ and resistivity $\rho(H, T)$ measurements on high quality single crystals of the light rare-earth diantimonides RSb_2 , $R = \text{La-Nd, Sm}$. All of these, excepting LaSb_2 , magnetically order at low temperatures, and for CeSb_2 and NdSb_2 several magnetically ordered phases were observed in low-field magnetization and zero-field resistivity measurements. For $R = \text{Ce-Sm}$ strong anisotropies, associated with crystalline electric field (CEF) splitting of the R^{3+} ion, were found in $M(T)$ measurements both below and above magnetic ordering temperatures. Furthermore, for $R = \text{Ce-Nd}$ metamagnetic transitions were observed in $M(H)$ and $\rho(H)$ for $H \parallel (ab)$ in the magnetically ordered state. In addition, above 15 kG de Haas-van Alphen oscillations are observed for SmSb_2 and Shubnikov-de Haas quantum oscillations are observed above ~ 120 kG for NdSb_2 and SmSb_2 . The zero-field in-plane resistivity ρ_{ab} of all of the compounds is metallic ($d\rho/dT > 0$), with residual resistance ratios ranging from 40 to 750. The c -axis resistivity is also metallic, but appears to be considerably larger than the in-plane value, consistent with the diantimonides being quasi-two-dimensional materials. The magnetoresistance of all members of the series is large, approximately linear in H at moderate fields, and is also dependent on the relative orientation of the applied magnetic fields to the crystallographic axes. The extreme case of SmSb_2 has $[\rho(55 \text{ kG}) - \rho(0)]/\rho(0) > 50\,000\%$ at $T = 2 \text{ K}$ and $H \parallel c$. [S0163-1829(98)03621-2]

I. INTRODUCTION

The light rare-earth diantimonides RSb_2 ($R = \text{La-Nd, Sm}$) all crystallize in the orthorhombic SmSb_2 structure.^{1,2} This highly anisotropic, layered structure has two unique Sb sites and one unique R site. One of the Sb sites forms two-dimensional (2D) sheets, the other Sb site and R site form slabs of triangular prisms that separate the Sb sheets. For heavier rare earths the diantimonides in the SmSb_2 structure are formed only as high-temperature-high-pressure, metastable phases.² Although the light rare-earth diantimonides were first synthesized several decades ago, little is known of the magnetic and transport properties of these compounds: superconductivity at $T_c \approx 0.4 \text{ K}$ was detected in LaSb_2 ;³ CeSb_2 was characterized as an anisotropic ferromagnet with $T_C = 15 \text{ K}$;⁴ PrSb_2 was found to be antiferromagnetic below $T_N = 5.1 \text{ K}$ with a metamagnetic transition at $H = 6.5 \text{ kG}$, $T = 1 \text{ K}$.⁵ In addition, recent studies of PrSb_2 (Refs. 6 and 7) revealed several metamagnetic transitions at low temperature, and found an anomaly in resistance at $T^* \approx 100 \text{ K}$, possibly originating from the charge- or spin-density wave and presented pressure dependencies of T_N , T^* , and the metamagnetic transitions in this material.

Successful growth of high quality single crystals of the light rare-earth diantimonides allows us to address several issues in the present work: (a) evolution of the (anisotropic) magnetic properties within the series with the change of the rare earth; (b) manifestation of the metamagnetic transitions in magnetization and magnetoresistance, and the temperature dependence of the metamagnetism in RSb_2 ; (c) anisotropic magnetoresistance of these layered compounds in the ordered and paramagnetic state.

The outline of the paper is as follows. After a brief review

of the experimental methods, we will present the experimental results starting with low-field (up to 55 kG) temperature- and field-dependent magnetization and resistivity for each of five light rare-earth diantimonides RSb_2 ($R = \text{La-Nd, Sm}$); followed by high-field magnetoresistance of LaSb_2 , NdSb_2 , and SmSb_2 . The experimental section is followed by a discussion, where we will try to reveal some trends in the magnetic properties within the series and to compare the results of our study of magnetoresistance with the existing theoretical views and results for some other quasi-two-dimensional materials.

II. EXPERIMENT

Large ($\sim 15 \times 15 \times 1 \text{ mm}^3$) single crystals of RSb_2 ($R = \text{La-Nd, Sm}$) were grown out of antimony flux.^{4,8} The crystals grow as soft plates with the c -axis perpendicular to the plates. The samples are micaceous, and layers can be easily peeled off. Each of these layers is malleable but, despite this ease of deformation, very high residual resistance ratios (several hundreds) are found in this family (see below). Due to the high malleability of the compounds, powder x -ray diffraction and even Laue diffraction are very difficult to perform. However, examination of the light rare-earth-antimony binary phase diagrams⁹ show unambiguously that the resulting crystals are indeed RSb_2 . Additionally, the RSb_2 stoichiometry is confirmed by the Curie-Weiss analysis of the high-temperature susceptibility (see below).

Magnetization measurements were performed using a commercial Quantum Design MPMS-5 superconducting quantum interference device (SQUID) magnetometer ($T = 1.8\text{--}350 \text{ K}$, $H_{\text{max}} = 55 \text{ kG}$) with the field aligned parallel or perpendicular to the c -axis of the crystals. The electrical

resistance was measured using a Linear Research LR-400 ac bridge, with a frequency of 16 Hz and a typical current density of $1\text{--}3\text{ A/cm}^2$. Electrical contact was made to the samples using EPOTEC H20E silver epoxy, and one of two contact configurations were used. The in-plane resistivity (ρ_{ab}) was measured using a standard four-probe technique for samples cut into bars approximately $6 \times 1 \times 0.2\text{ mm}^3$ with current contacts on each end of the sample and two voltage contacts along the length (see the right inset to Fig. 2). The c -axis resistivity was estimated from measurements using a modified four-probe configuration. In this case, small samples with approximately $2 \times 2\text{ mm}^2$ in-plane dimensions and $0.5\text{--}1\text{ mm}$ thickness were contacted with dotlike voltage contacts in the centers of the opposite planes, with a wide ‘‘U’’-shaped current contacts covering more than half of the surface of the plates (see the left inset to Fig. 2). It should be noted that the modified contact geometry used for ρ_c measurements requires that $\rho_c \gg \rho_{ab}$ so as to establish a uniform current path (i.e., the equivalent isotropic crystal must be substantially longer along the c -axis than the in-plane dimensions) and this concern is returned to later. Furthermore, it is noted that magnetoresistance measurements using the modified contact geometry may suffer from Hall voltage contributions. However, despite these reservations, we were able to obtain estimates of the c -axis resistivity of LaSb₂ and SmSb₂.

Both in-plane and c -axis magnetoresistance were measured in the H - T environment of the MPMS-5 SQUID magnetometer, with the field aligned either parallel or perpendicular to the current for longitudinal and transverse measurements, respectively. In addition, for LaSb₂, NdSb₂, and SmSb₂, high-field transverse magnetoresistance measurements [$H \parallel c$, $I \parallel (ab)$] from 1.5 to 100 K were performed utilizing a 200 kG superconducting magnet at the National High Magnetic Field Laboratory-Los Alamos Facility. Finally, it is noted that resistivity measurements were performed on single crystals from different batches as well as on different samples from the same batch, leading to the different residual resistance ratios for specific samples as described in later sections.

III. RESULTS

A. Low-field measurements

1. LaSb₂

Figure 1 shows anisotropic susceptibility of LaSb₂. The magnetization isotherms $M(H)$ (Fig. 1, inset) are practically linear with field, almost isotropic, and do not show any anomaly up to 55 kG. The susceptibility characterizes LaSb₂ as a weakly temperature-dependent isotropic diamagnet. The in-plane resistivity (Fig. 2) has metallic behavior ($d\rho/dT > 0$) with $\rho(T)$ linear for $T > 50\text{ K}$. The high value of the residual resistance ratio ($\text{RRR} = \rho(300\text{ K})/\rho(2\text{ K}) \approx 59$) indicates the high quality of the samples. No traces of superconductivity were observed down to 1.8 K, consistent with earlier measurements of $T_c = 0.4\text{ K}$.³ For LaSb₂ the resistivity with the current flowing along the c -axis (Fig. 2), ρ_c , at 300 K is more than an order of magnitude higher than ρ_{ab} and $\text{RRR} \approx 12$ is substantially lower than observed for ρ_{ab} . In addition, at approximately 260 K, a smeared anomaly in the

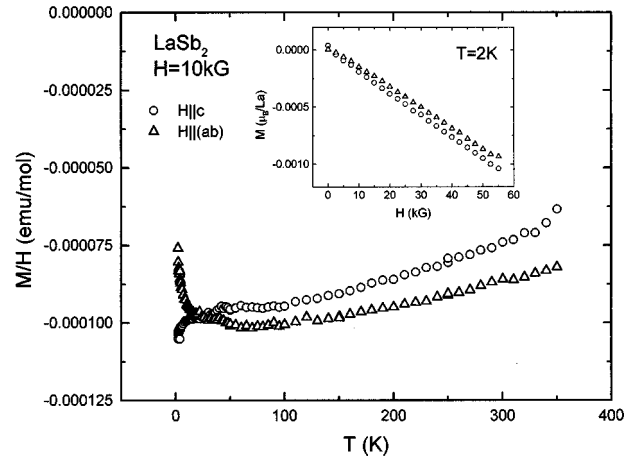


FIG. 1. Anisotropic susceptibility of LaSb₂. Inset: anisotropic magnetization isotherms for LaSb₂ at $T = 2\text{ K}$.

resistivity is observed, which is much less pronounced for $I \parallel (ab)$ (Fig. 2). Magnetoresistance of LaSb₂ is positive [Fig. 3(a)] and $\Delta\rho(H)$ is close to linear in H [more careful analysis shows that for LaSb₂ it approximately follows the power law $\Delta\rho(H) \propto H^\alpha$ with $\alpha \approx 1.1\text{--}1.3$.] The approximate slopes, defined here as $s(T) = 1/55\text{ kG} [\rho(T, 55\text{ kG}) - \rho(T, 0)]/\rho(T, 0)$ are listed in Table I. In-plane magnetoresistance is anisotropic in the field direction with $\Delta\rho_{ab}(H \parallel c) > \Delta\rho_{ab}(H \parallel (ab))$. This anisotropy is more pronounced at low temperature, but it persists up to 100–150 K. c -axis magnetoresistance $\Delta\rho_c(H)$ [Fig. 3(b)] is qualitatively similar to the in-plane magnetoresistance $\Delta\rho_{ab}(H)$, although the difference in the c -axis magnetoresistance for $H \parallel c$ and $H \parallel (ab)$ is much smaller than in the case of $I \parallel (ab)$. The anisotropy in the c -axis magnetoresistance also persists up to high temperatures. For the fields $H > 5\text{--}10\text{ kG}$ the c -axis magnetoresistance is close to linear in magnetic field. The approximate slopes of the field-dependent magnetoresistance are listed in Table I.

2. CeSb₂

Anisotropic susceptibility and zero-field electrical resistivity of CeSb₂ are presented in Fig. 4 and Fig. 5. This set of

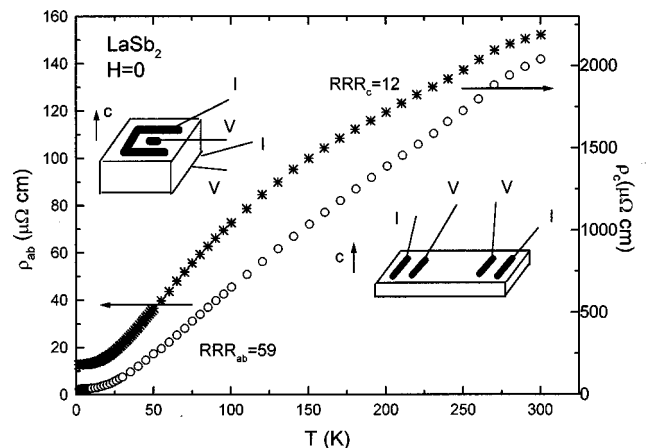
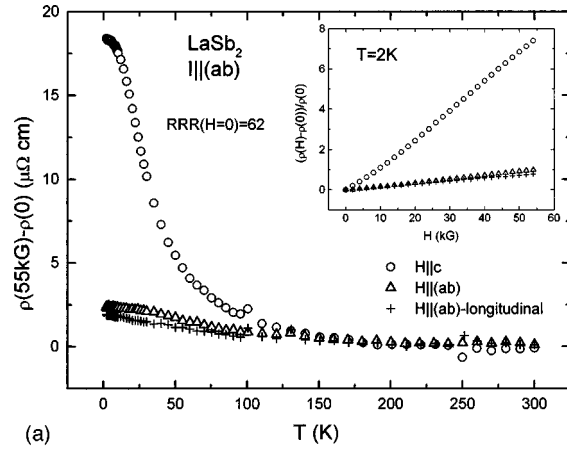
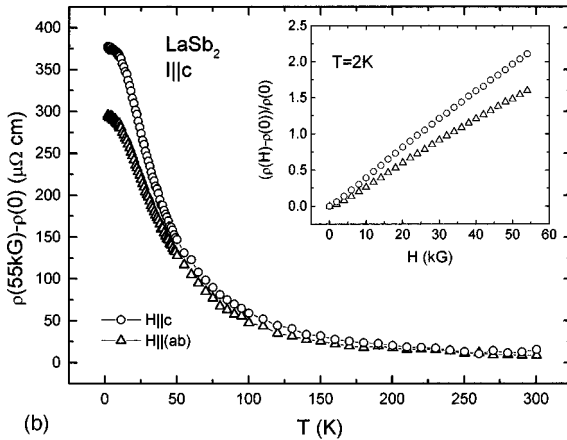


FIG. 2. Zero-field resistivity of LaSb₂, $I \parallel (ab)$ [open circles] and $I \parallel c$ [double crosses]. Note different Y scales on the graph. Insets show contact configuration for two measurement geometries.



(a)



(b)

FIG. 3. (a) Temperature dependence of magnetoresistance of LaSb_2 at 55 kG, $I\parallel(ab)$, inset: anisotropic magnetoresistance of LaSb_2 at 2 K; (b) Temperature dependence of magnetoresistance of LaSb_2 at 55 kG, $I\parallel c$, inset: anisotropic magnetoresistance of LaSb_2 at 2 K.

the data is in general agreement with the results of Ref. 4. The susceptibility (Fig. 4) is anisotropic, the with the c -axis being the hard magnetization axis. For $T \geq 150$ K the inverse susceptibility is nearly linear in temperature, and it extrapolates to a positive value of $\Theta_p^{ab} \approx 26$ K for the magnetic field applied in the (ab) plane, and negative $\Theta_p^c \approx -170$ K for the field along c -axis. The polycrystalline average of magnetic

TABLE I. Approximate slopes of the magnetoresistance in RSb_2 ($R=\text{La, Pr, Nd, Sm}$). For PrSb_2 and NdSb_2 data for $H\parallel(ab)$, $I\parallel(ab)$ at $T=2$ K are omitted due to spurious contributions in magnetoresistance at metamagnetic transitions. For $I\parallel c$ measurements only for LaSb_2 and SmSb_2 were performed.

RSb_2	$s = 1/55 \text{ kG} [\rho(55 \text{ kG}) - \rho(0)] / \rho(0) [10^{-2} \text{ kG}^{-1}]$							
	$I\parallel(ab)$				$I\parallel c$			
	$T=2 \text{ K}$		$T=20 \text{ K}$		$T=2 \text{ K}$		$T=20 \text{ K}$	
R	$H\parallel c$	$H\parallel(ab)$	$H\parallel c$	$H\parallel(ab)$	$H\parallel c$	$H\parallel(ab)$	$H\parallel c$	$H\parallel(ab)$
La	18	1.8	5.9	0.9	4	3	2.5	2
Pr	26		3.2	0.2				
Nd	138		3.6	0.9				
Sm	970	24	3.5	0.9	18	40	1.5	4.5

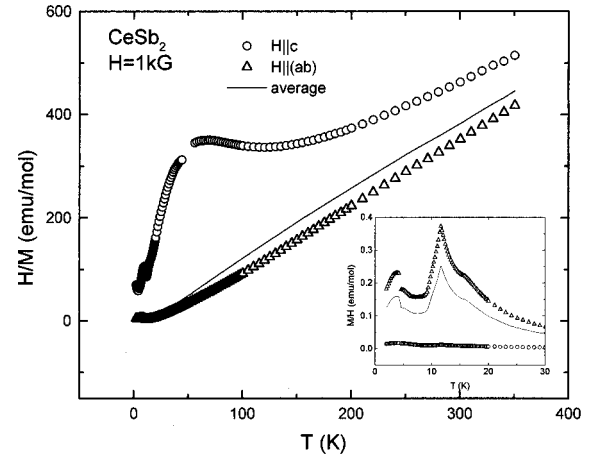


FIG. 4. Inverse susceptibility of CeSb_2 , inset: low-temperature susceptibility.

susceptibility [approximated by $\chi_{av} = (\chi_c + 2\chi_{ab})/3$] gives an effective magnetic moment of $\mu_{\text{eff}} \approx 2.63 \mu_B/\text{Ce}$. The temperature-dependent resistivity (Fig. 5) resembles that observed in Kondo-lattice compounds, and has $\text{RRR} \approx 94$. The low-temperature behavior of CeSb_2 is quite complicated with three anomalies (at 15.5, 11.7, and 9.3 K) clearly visible in the derivative of the resistivity $d\rho/dT$ and the magnetization $d(MT)/HdT$ (both shown in the inset of Fig. 5). In addition, a broad maximum centered around 2.6 K is observed in $d(MT)/HdT$ that has no corresponding feature in $\rho(T)$ and the origin of this anomaly is unclear. The present study of the low-temperature behavior of CeSb_2 is more detailed than the one performed in Ref. 4. In Ref. 4 a ferromagnetic ground state with $T_C = 15$ K was suggested for CeSb_2 , and a slight anomaly at ~ 12 K in the resistivity vs temperature curve was mentioned without an indication of the corresponding anomaly in magnetization. Taken together, resistivity and magnetization data suggest that CeSb_2 passes through a sequence of *at least* three magnetically ordered states at low temperatures and zero magnetic field.

Field-dependent magnetization isotherms $M(H)$ for CeSb_2 are shown in Fig. 6(a). For $H\parallel(ab)$ metamagnetic transitions are clearly visible. The shape of the $M(H)$ curve at $T=2$ K suggests that different spin-ordering processes oc-

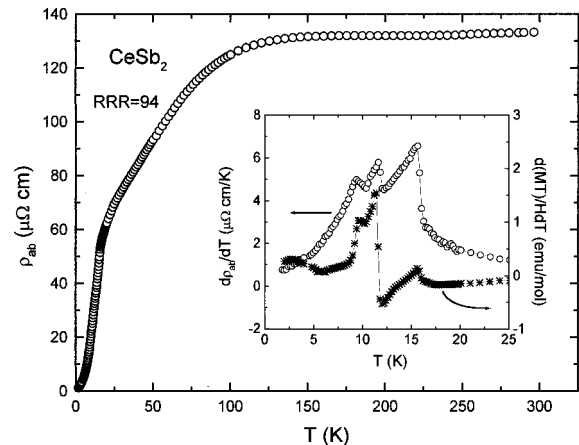


FIG. 5. Zero-field resistivity of CeSb_2 , $I\parallel(ab)$. Inset: temperature derivatives of resistivity and $(\chi_{\text{dc}}T) [H\parallel(ab)]$ for CeSb_2 .

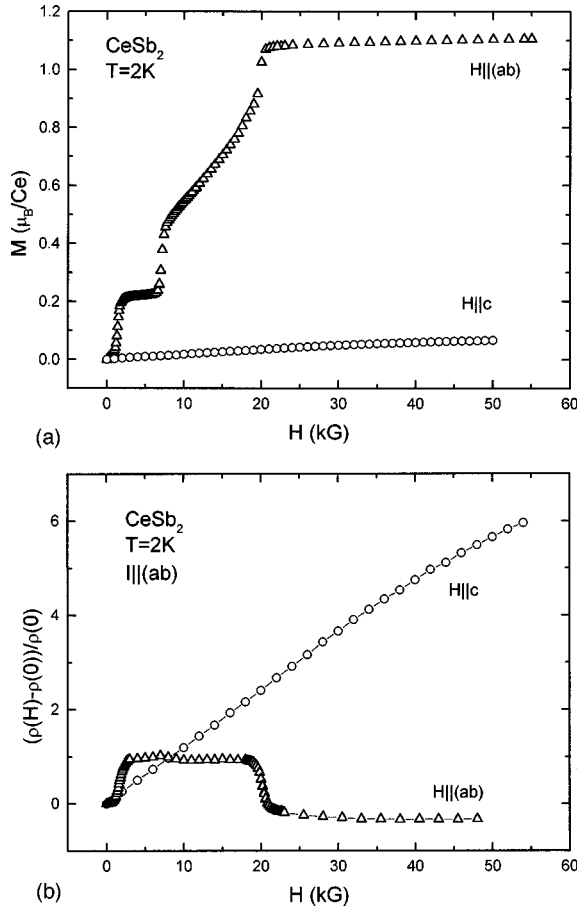


FIG. 6. (a) Anisotropic magnetization isotherms for CeSb_2 at $T = 2$ K. (b) Anisotropic magnetoresistance of CeSb_2 at $T = 2$ K.

cur in CeSb_2 with increasing magnetic field. While the two, lower-field, sharp metamagnetic transitions are possibly associated with some kind of spin-flip processes, the change of magnetization associated with the next transition is gradual and may be due to the rotation of the spins, so it is possible that the ordered phase formed as a result of the second metamagnetic transition has some fan-type structure. Metamagnetic transitions manifest themselves not only in field-dependent magnetization but also in magnetoresistance. Fig. 6(b) shows the anisotropic magnetoresistance of CeSb_2 . It is clearly seen that sharp changes in resistivity as a function of applied magnetic field occur exactly at the same fields as do the changes in magnetization [note that due to anticipated in-plane anisotropy of the metamagnetic transitions, care was taken to perform both these measurements for the same (although arbitrary) orientation of the magnetic field in the (ab) plane]. Based on the measurements of magnetization and magnetoresistance as a function of temperature and magnetic field [Figs. 7(a) and 7(b)], a tentative H - T phase diagram for CeSb_2 for one direction of the magnetic field in the (ab) plane was constructed [Fig. 7(c)] as an example of the complexity of the magnetic order in the light rare-earth diantimonides. There appear to be at least four magnetically ordered phases labeled I–IV. It should be noted that for fields greater than 2.5 kG, phases III and IV no longer exist, making careful, low-field measurements of these states essential.

At temperatures between 20–100 K (above the magnetic ordering for CeSb_2) both transverse and longitudinal magnetoresistance for $H \parallel (ab)$ are negative and quite high $\{[\rho(20 \text{ K}, 55 \text{ kG}) - \rho(20 \text{ K}, 0)] / \rho(20 \text{ K}, 0) \approx -35\%$ while the transverse magnetoresistance for $H \parallel c$ is smaller and positive (Fig. 8). For $H \parallel (ab)$ $\Delta\rho(H) \propto H^2$ and this behavior is reminiscent of that for heavy fermion and Kondo-lattice compounds,^{10,11} including the anisotropy of magnetoresistance that was observed, for example, at relatively high temperatures in CeCu_6 .¹²

3. PrSb_2

The magnetization of PrSb_2 is anisotropic (Fig. 9) with the c axis being the hard magnetization axis. For $T < T_N = 5.1$ K, PrSb_2 appears to be in an antiferromagnetic ground state, and the value of T_N is consistent with previous^{2,6,7} data. At high temperatures the inverse susceptibility is linear in temperature, with $\Theta_p^c \approx -75.8$ K and $\Theta_p^{ab} \approx 22$ K, while the polycrystalline average of the susceptibility gives a value for the effective moment of $\mu_{\text{eff}} \approx 3.55 \mu_B / \text{Pr}$. As can be seen in Fig. 10(a) the residual resistance ratio of PrSb_2 is 42. The zero-field resistivity drops abruptly for $T < 5.1$ K due to the loss of spin-disorder scattering in the antiferromagnetic ordered state. In addition, just before the antiferromagnetic transition, $\rho(T)$ has a slight upturn, which may be due to the formation of a superzone gap at the Fermi surface due to antiferromagnetic ordering.¹³ A further anomaly in $\rho(T)$ occurs at $T \approx 100$ K,⁷ though there is no corresponding anomaly in magnetization measurements. Similar humplike anomalies have been observed in the resistivity of Cr and its alloys¹⁴ (and other materials), in which case it is a signature of a phase transition associated with spin- or charge-density wave. Magnetic fields up to 55 kG do not change the position of the anomaly [Fig. 10(b)], which makes a charge-density wave a somewhat more favorable hypothesis.

In PrSb_2 , a series of metamagnetic transitions were observed at low temperatures.^{5–7} The $M(H)$ curve at $T = 2$ K for $H \parallel (ab)$ [Fig. 11(a)] shows two clear metamagnetic transitions, while for $H \parallel c$ a smeared feature in $M(H)$ is observed, suggesting that a metamagnetic transition with the critical field $H_c \approx 17$ kG occurs in this orientation as well, or, alternatively, about 5% of the sample is misaligned [$H \parallel (ab)$]. Field-dependent magnetoresistance is shown in Fig. 11(b). For $H \parallel (ab)$ clear anomalies associated with the metamagnetic transitions are observed with the critical fields in agreement with the magnetization measurements. For $H \parallel c$ magnetoresistance is positive and quite high with possible smeared features. $M(H)$ measurements for the different in-plane directions of the magnetic field as well as for H along the c axis reveal that the complete picture of metamagnetism in the diantimonides, possessing orthorhombic symmetry, is extremely complicated. The full angular dependence of metamagnetism in these compounds will be a subject of another study.

Temperature-dependent magnetoresistance $\rho(T, 55 \text{ kG}) - \rho(T, 0)$ (Fig. 12) is anisotropic. For the transverse magnetoresistance with $H \parallel c$ the effect of field is higher and does not involve additional complications due to metamagnetism in this field range. A steep increase of $\rho(T, 55 \text{ kG}) - \rho(T, 0)$ is observed for the temperatures below the zero-field value of the magnetic ordering temperature, and the magnetoresis-

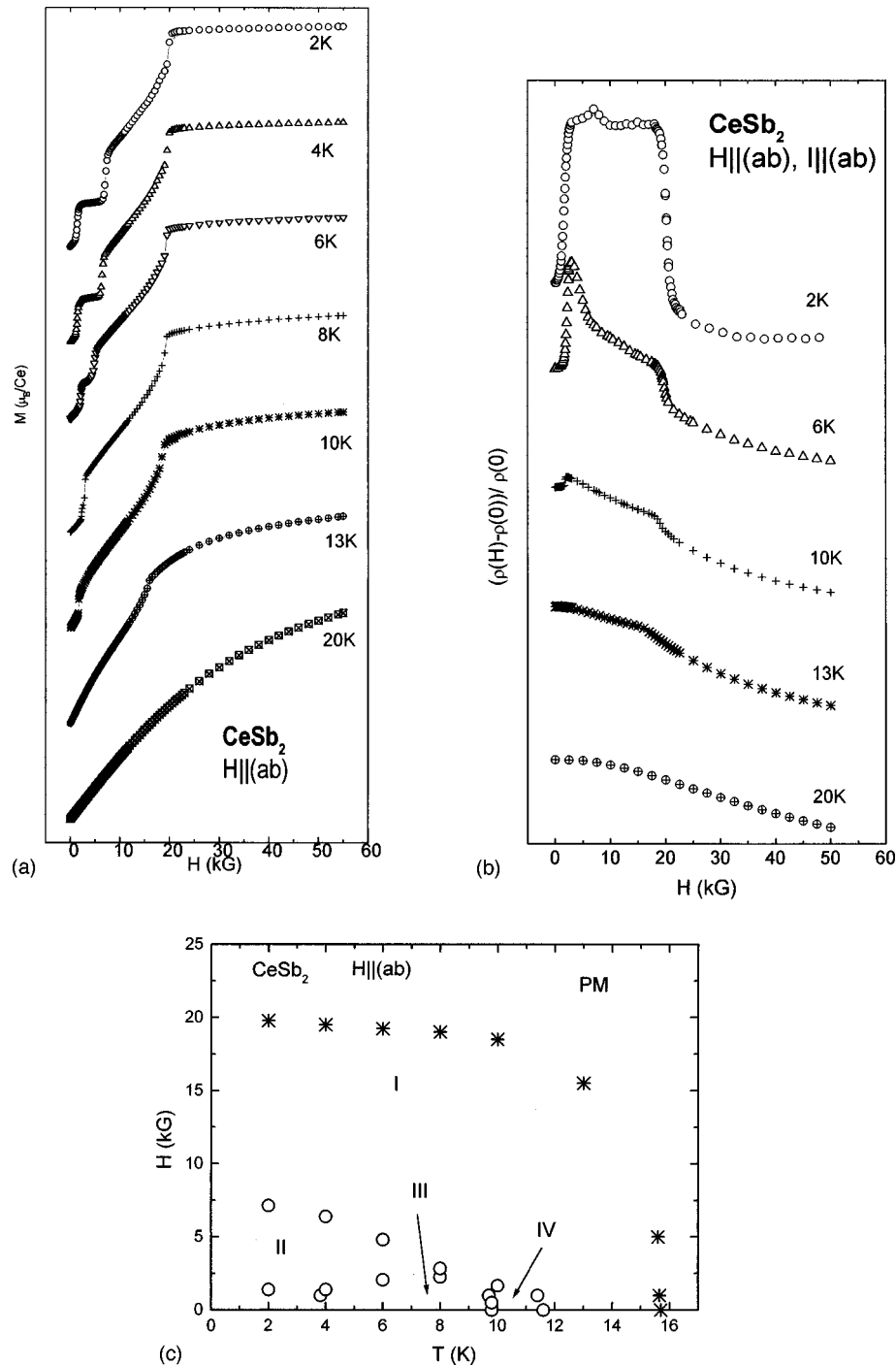


FIG. 7. (a) In-plane field-dependent magnetization for CeSb_2 at different temperatures. (b) In-plane field-dependent magnetoresistance for CeSb_2 at different temperatures. (c) Tentative H - T phase diagram for $H \parallel (ab)$ in CeSb_2 .

tance in the ordered state is significantly higher than in the paramagnetic state. It should be noted that for PrSb_2 ($H \parallel c$) (Fig. 12) there is an additional maximum in $\rho(T, 55 \text{ kG}) - \rho(T, 0)$ that occurs at temperatures around 15 K, well separated from the magnetic ordering temperature (5.1 K) and the anomaly at $T^* \approx 100 \text{ K}$ [Fig. 10(a)], neither of which is shifting with the fields up to 55 kG.

4. NdSb_2

NdSb_2 is another example of a complex sequence of magnetically ordered states at low temperatures (Figs. 13 and 14). Two magnetic transitions (at 8 and 6 K) are clearly seen

both in $d\rho/dT$ and $d(MT)/HdT$ data (Fig. 15), another anomaly (at 2.3 K) is present in $d(MT)/HdT$ and raw M/H vs T data (Fig. 13, inset) but is not clear in $d\rho/dT$. The magnetic susceptibility is anisotropic (c -hard magnetization axis), and the inverse susceptibility is linear in temperature. It gives $\Theta_p^c \approx -59.1 \text{ K}$ and $\Theta_p^{ab} \approx -16.2 \text{ K}$. The value of the effective moment from the polycrystalline average is $3.68 \mu_B/\text{Nd}$. The residual resistance ratio for NdSb_2 is 127, and the zero-field electrical resistivity has a humplike anomaly at $\sim 38 \text{ K}$, similar to the one in PrSb_2 at 100 K. As in PrSb_2 , this anomaly may originate from some kind of density wave.

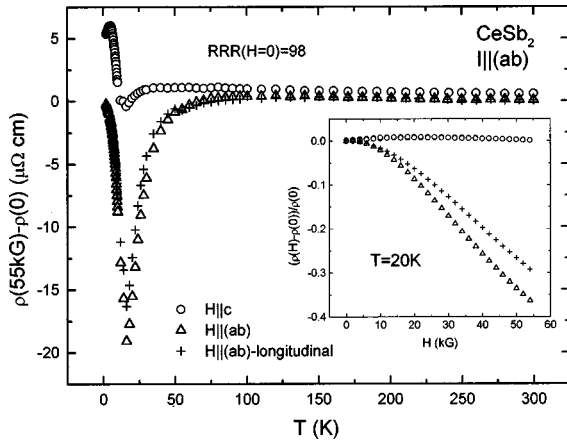


FIG. 8. Temperature dependence of magnetoresistance of CeSb_2 at 55 kG, $I\parallel(ab)$, inset: anisotropic magnetoresistance of CeSb_2 at 20 K.

In-plane metamagnetism was also observed in NdSb_2 [Fig. 16(a)]. Again, it is anisotropic and the saturated magnetization state does *not* seem to be achieved for fields up to 55 kG. For one of the in-plane directions [“*B*” in Fig. 16(a), where the angle between “*A*” and “*B*” is approximately 45°] the field-dependent magnetization is close to the magnetization for $H\parallel c$. This suggests extremely strong in-plane anisotropy, with the metamagnetic transitions, if they exist for H along “*B*,” shifted to the fields above our experimental limits. Field-dependent magnetoresistance at $T=2$ K [Fig. 16(b)] is high and close to linear in field for $H\parallel c$ and confirms the existence of the metamagnetic transitions for $H\parallel(ab)$ [the applied field direction for the transverse magnetoresistance measurements in Fig. 16(b) coincides with the “*A*” direction in Fig. 16(a)]. The overall behavior of the temperature-dependent magnetoresistance of NdSb_2 (Fig. 17) is similar to that of PrSb_2 , although the maximum at $T \approx 15$ K in $\rho(T, 55 \text{ kG}) - \rho(T, 0)$ for $H\parallel c$ is absent.

5. SmSb_2

The magnetic susceptibility of SmSb_2 is anisotropic and shows an anomaly at $T_N = 12.5$ K (Fig. 18, inset). In the ordered state the c axis is a hard magnetization axis, however,

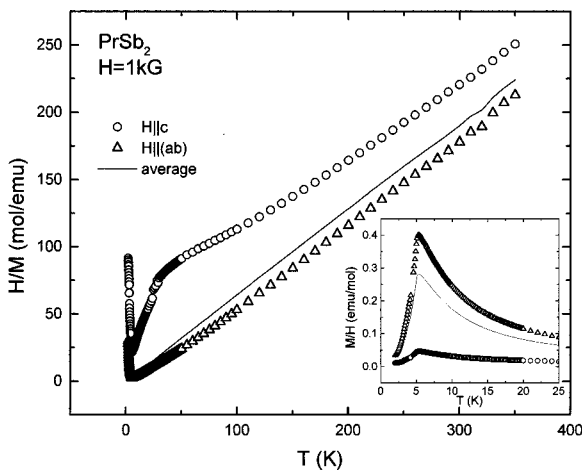
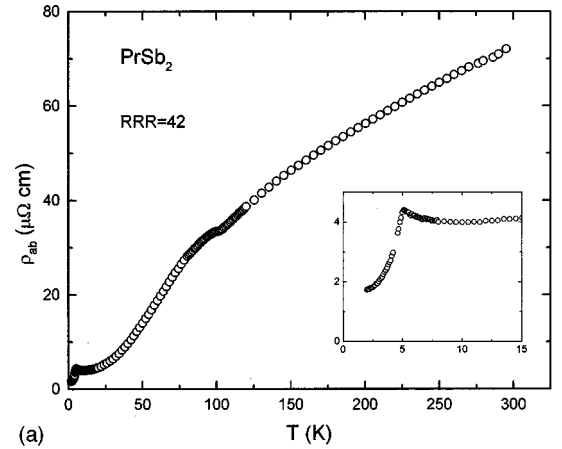
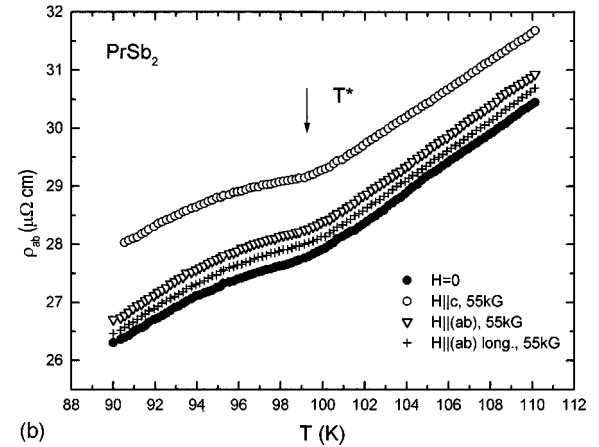


FIG. 9. Inverse susceptibility of PrSb_2 , inset: low-temperature susceptibility.



(a)



(b)

FIG. 10. (a) Zero-field resistivity of PrSb_2 , $I\parallel(ab)$. Inset: enlarged low-temperature part. (b) $T^* \approx 100$ K anomaly in resistivity of PrSb_2 : effect of 55 kG field applied in different directions.

in contrast to the other magnetic light rare-earth diantimonides, the anisotropy of the magnetic susceptibility changes several times with temperature. The inverse susceptibility is nonlinear in temperature (Fig. 18), and at high temperatures it has a tendency to saturate, which corresponds to the temperature-independent susceptibility of Sm^{2+} . The slope of M/H vs T between 30 and 100 K is somewhat lower than that expected for Sm^{3+} . Probably, as in some other intermetallic compounds,¹⁵ Sm in SmSb_2 has its valence fluctuating between $3+$ and $2+$. Zero-field resistivity of SmSb_2 is metallic ($d\rho/dT > 0$) for current flowing in the (ab) plane and along the c axis (Fig. 19). SmSb_2 has the highest residual resistance ratio: $\text{RRR} \approx 415$ for $I\parallel(ab)$, for the current flowing along the c axis $\text{RRR} \approx 130$. Both in-plane and c -axis zero-field resistivity exhibits a sharp drop associated with the loss of spin-disorder scattering (Fig. 19) at the same temperature as the anomaly in the magnetic susceptibility.

The magnetization isotherms $M(H)$ for SmSb_2 are shown in Fig. 20(a). The magnetization is anisotropic and linear in field up to 55 kG. For $H\parallel c$, de Haas-van Alphen oscillations are observed for $H \geq 15$ kG and for temperatures up to at least 9 K. The spectrum of these oscillations at $T=2$ K in the field range $40 \text{ kG} \leq H \leq 55 \text{ kG}$ [Fig. 20(b), inset] is presented in Fig. 20(b). Four frequencies corresponding to small parts of the Fermi surface are clearly seen in the spectrum. Analy-

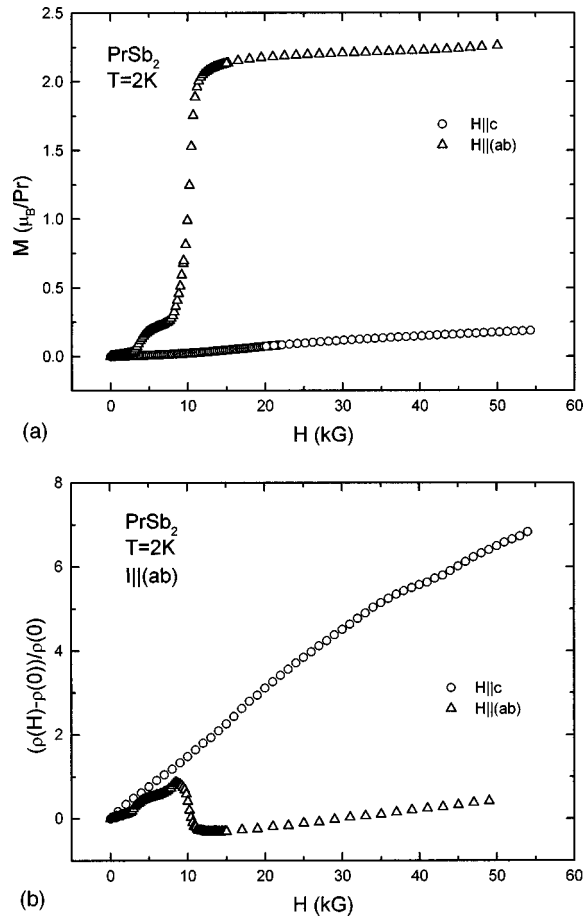


FIG. 11. (a) Anisotropic magnetization isotherms for PrSb_2 at $T=2$ K. (b) Anisotropic magnetoresistance of PrSb_2 at $T=2$ K.

sis of the oscillations at different temperatures and in different field ranges yields estimations of the effective masses associated with the observed orbits and so-called Dingle temperature T_D , which is a characteristic of an impurity scattering.¹⁶ The results are presented in Table II. The frequency $F4$ is probably the second harmonic of $F3$. Indeed, $F4=2 * F3$ and within experimental accuracy $m^*(F4) \approx 2 * m^*(F3)$, which is expected in the Lifshits-Kosevich

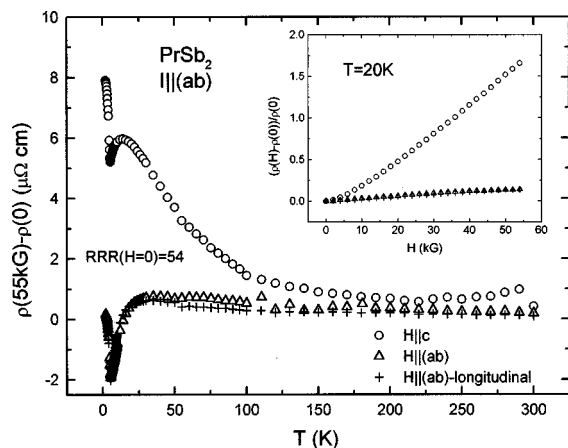


FIG. 12. Temperature dependence of magnetoresistance of PrSb_2 at 55 kG, $I \parallel (ab)$, inset: anisotropic magnetoresistance of PrSb_2 at 20 K.

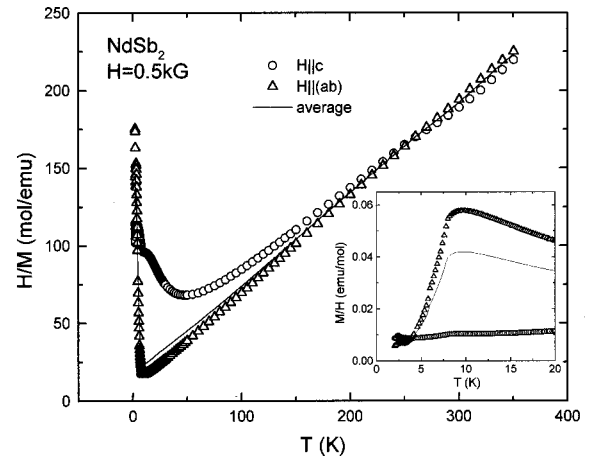


FIG. 13. Inverse susceptibility of NdSb_2 , inset: low-temperature susceptibility.

description of the quantum oscillations in metals.¹⁷ The situation with the $F1$ and $F2$ frequencies is more complicated. The frequency $F2$ is two times higher than $F1$, however the value of the effective mass $m^*(F2)$ is lower or close to $m^*(F1)$ but not $2 * m^*(F1)$. These deviation from the Lifshits-Kosevich description may suggest that $F2$ is a second harmonic of the $F1$ fundamental frequency resulting from magnetic interaction between the electrons (Shoenberg effect).¹⁶ A detailed study of the de Haas-van Alphen and Shubnikov-de Haas quantum oscillations in SmSb_2 at temperatures down to 400 mK and in magnetic field up to 500 kG will be presented elsewhere.¹⁸

The temperature dependence of the magnetoresistance of SmSb_2 for $I \parallel (ab)$ [Fig. 21(a)] is qualitatively similar to that of NdSb_2 (Fig. 17). At $T=2$ K the relative change of resistivity in the applied field of 55 kG exceeds 500 [Fig. 21(a), inset]. For SmSb_2 , the $I \parallel c$ magnetoresistance is anisotropic [Fig. 21(b)] but the anisotropy is somewhat smaller and is reversed both in the ordered and paramagnetic state, as compared to the case of $I \parallel (ab)$. The approximate slopes of magnetoresistance at 2 and 20 K for $I \parallel (ab)$ and $I \parallel c$ are listed in Table I. Magnetoresistance remains anisotropic up to high

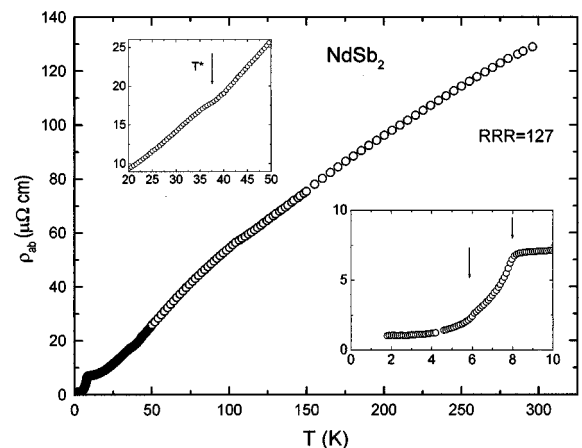


FIG. 14. Zero-field resistivity of NdSb_2 , $I \parallel (ab)$. Insets: enlarged low-temperature part; enlarged region around the anomaly at T^* .

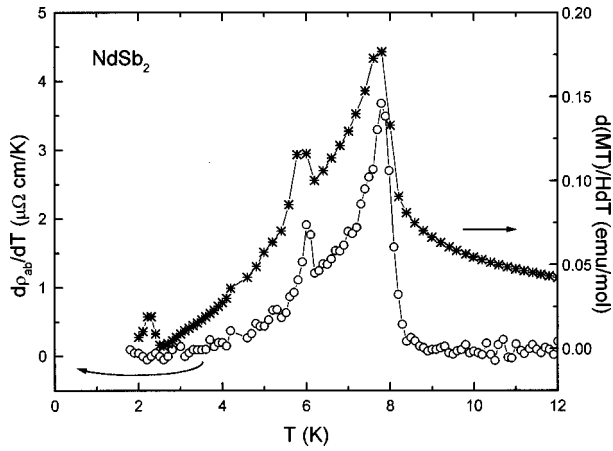


FIG. 15. Temperature derivatives of resistivity and $(\chi_{DC}T)$ [$H||ab$] for $NdSb_2$.

temperatures. Finally, it has to be mentioned that in the case of $I||c$ the magnetoresistance measured using the modified contact geometry (as described previously) may have significant contributions due to Hall voltages, so the magnetoresistance data for current flowing along the c axis give a semi-quantitative description of these materials rather than exact results.

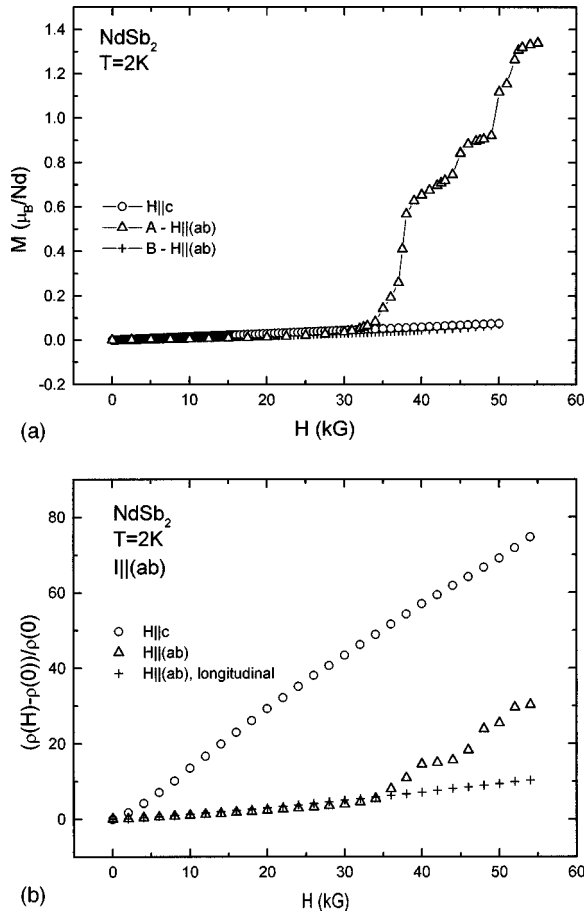


FIG. 16. (a) Anisotropic magnetization isotherms for $NdSb_2$ at $T=2$ K (the angle between the orientations “A” and “B” is approximately 45°). (b) Anisotropic magnetoresistance of $NdSb_2$ at $T=2$ K.

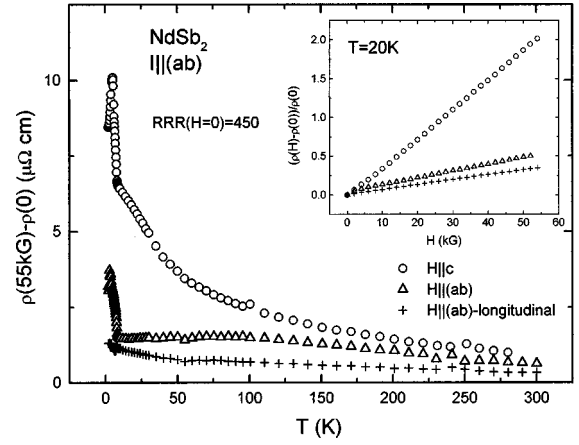


FIG. 17. Temperature dependence of magnetoresistance of $NdSb_2$ at 55 kG, $I||ab$, inset: anisotropic magnetoresistance of $NdSb_2$ at 20 K.

B. High-field magnetoresistance

$LaSb_2$ shows a striking feature in high ($H > 55$ kG) fields. As seen in Fig. 22, the zero-field resistance shows a monotonic decrease of scattering as the temperature decreases. However, by applying a magnetic field (along the c axis) a pronounced maximum is observed, moving up to 23 K at 180 kG. This maximum resembles the one observed in magnetoresistance $\rho(T, 55 \text{ kG}) - \rho(T, 0)$ for $PrSb_2$ ($H||c$) (Fig. 12). Since no magnetic transition was observed in $LaSb_2$ down to the lowest temperature investigated, the possible origin of this magnetic-field-induced anomaly requires more studies. Due to the two-dimensional character of this material, the possibility of this transition being a magnetic-field-induced density wave transition¹⁹ is currently under investigation.

In $NdSb_2$, a large transverse magnetoresistance ($H||c$) is observed at low temperatures [Fig. 23(a)]. It is interesting to note that the “break” in the resistivity (at the zero field T_N) does not move with the application of a large magnetic field. Figure 23(b) shows the transverse magnetoresistance (for $H||c$) at 2 and 20 K. An inflection point is observed at low temperature at 100 kG, which could be due to a metamagnetic-like transition. This transition disappears at 20 K. Shubnikov-de Haas oscillations are also observed in the

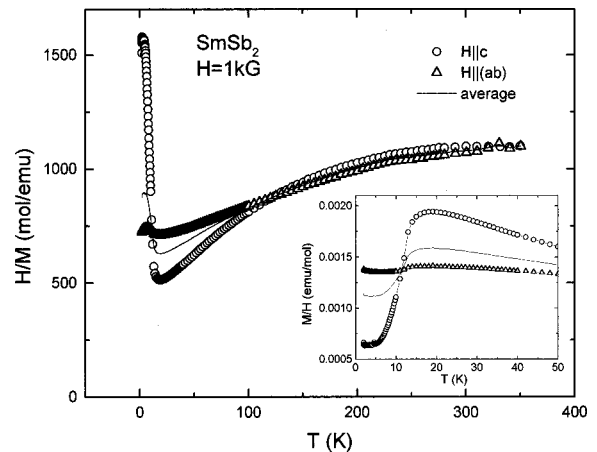


FIG. 18. Inverse susceptibility of $SmSb_2$, note absence of the Curie-Weiss behavior. Inset: low-temperature susceptibility.

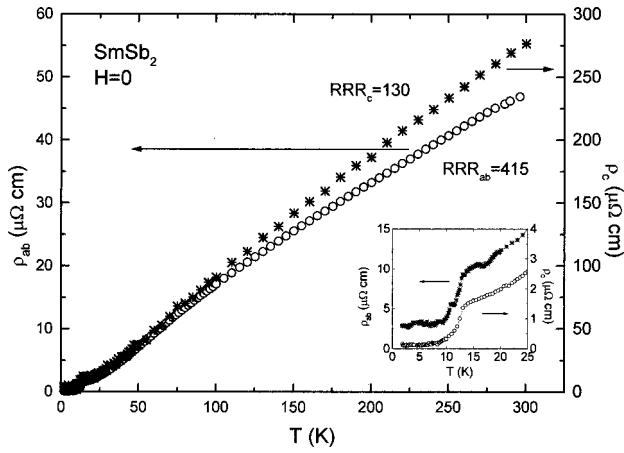


FIG. 19. Zero-field resistivity of SmSb_2 , $I \parallel (ab)$ [open circles] and $I \parallel c$ [double crosses]. Note different Y scales on the graph. Inset: enlarged low-temperature part.

transverse magnetoresistance at 2 K above 120 kG. A power spectrum of the data using maximum entropy method reveals two well-defined frequencies at 1 and 7.05 MG [Fig. 23(b), inset].

Figure 24(a) shows the transverse magnetoresistance ($H \parallel c$) as a function of temperature for SmSb_2 . The large

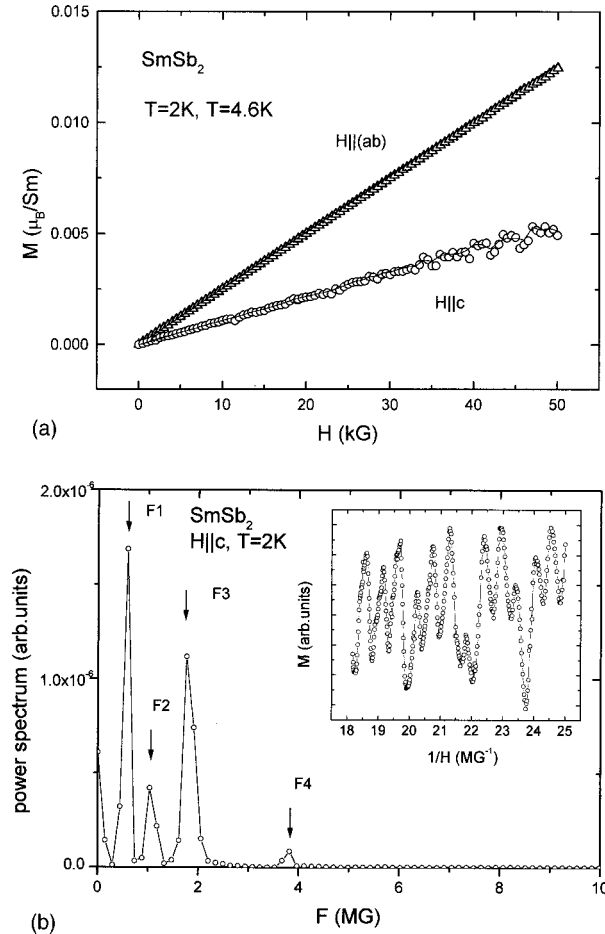


FIG. 20. (a) Anisotropic magnetization isotherms for SmSb_2 at $T=2$ K (symbols) and $T=4.6$ K (lines). (b) Spectrum of de Haas-van Alphen oscillations at $T=2$ K, $H \parallel c$ in SmSb_2 , inset: example of the de Haas-van Alphen oscillations in SmSb_2 .

TABLE II. Characteristics of the de Haas-van Alphen orbits in SmSb_2 for $H \parallel c$ (error in m^*/m_0 is 15–20%).

Frequency	F (MG)	m^*/m_0	T_D (K)
$F1$	0.56	0.17	2.0
$F2$	1.05	0.14	1.5
$F3$	1.82	0.18	2.4
$F4$	3.78	0.3	2.3

increase of the resistance at low temperatures in high magnetic fields is qualitatively similar to that seen in Fig. 23(a) for NdSb_2 at comparable applied fields. The field dependence of the transverse magnetoresistance ($H \parallel c$) at 1.5 K is shown in Fig. 24(b). An extremely large increase of magnetoresistance observed at this temperature is followed by the turn to saturation above ≈ 140 kG and, further, by Shubnikov-de Haas oscillations. Recent measurements¹⁸ in this compound up to 500 kG and down to 420 mK in temperature also indicated a maximum in the transverse magnetoresistance at around 200 kG followed by very strong oscillations. The frequencies of de Haas-van Alphen and Shubnikov-de Haas oscillations in SmSb_2 observed in high fields¹⁸ are consistent with the de Haas-van Alphen frequencies values obtained

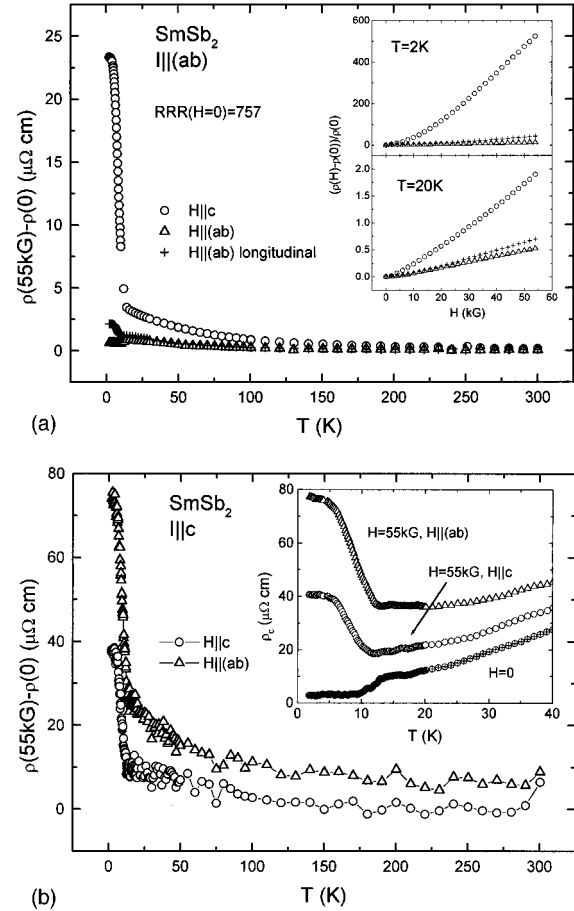


FIG. 21. (a) Temperature dependence of magnetoresistance of SmSb_2 at 55 kG, $I \parallel (ab)$, insets: anisotropic magnetoresistance of SmSb_2 at 2 and 20 K. (b) Temperature dependence of magnetoresistance of SmSb_2 at 55 kG, $I \parallel c$, inset: low-temperature out-of-plane resistivity of SmSb_2 in zero and 55 kG applied field.

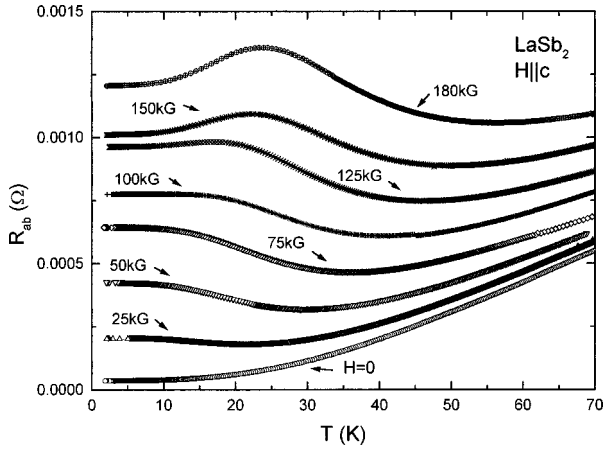


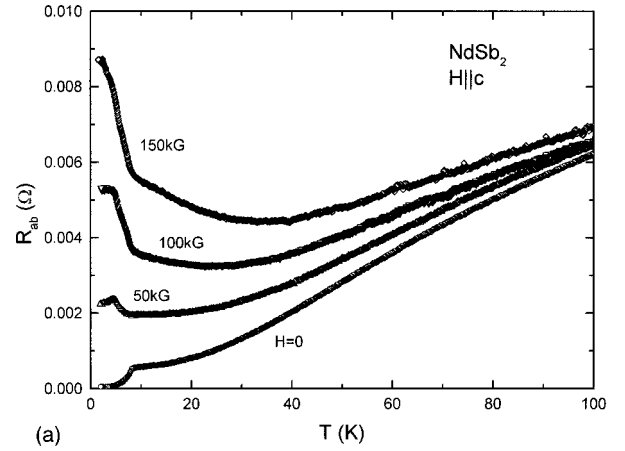
FIG. 22. High-field temperature-dependent transverse magnetoresistance of LaSb_2 ; $I \parallel (ab)$, $H \parallel c$.

from our field-dependent magnetization measurements (Table II). The values of Shubnikov-de Haas frequencies observed in NdSb_2 are very close to the quantum oscillation frequencies found in SmSb_2 , which suggests that these two materials have very similar Fermi surfaces. The fact that the spectrum of the oscillations in SmSb_2 is richer than in NdSb_2 may point to the differences in the details of the band structure, however a more plausible explanation is that the crystals of SmSb_2 are of higher quality (compare, for example, the values of RRR cited in Sec. III A 1) so the oscillations of some frequencies in NdSb_2 are smeared and not detectable.

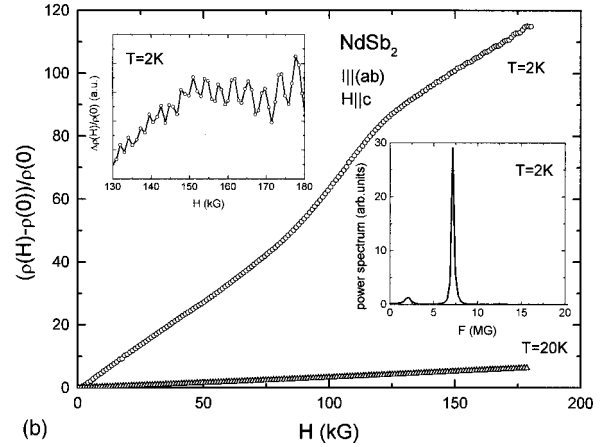
High-field magnetoresistance measurements confirm the steep increase of $\rho(T, H) - \rho(T, 0)$ (for $H \parallel c$), mentioned earlier, in RSb_2 , $R = \text{Pr, Nd, Sm}$ [Figs. 12, 17, and 21(a)] for the temperatures lower than zero-field magnetic ordering transition. High-field data (Figs. 23 and 24) clearly show that at low temperatures with applied field we have a continuous change in $\rho(T)$ from a decrease of the resistivity due to the loss of spin-disorder scattering in the magnetically ordered state in zero field to a gain in resistivity at temperatures below the ordering temperature in applied field. This effect is so large that for SmSb_2 that the resistivity at 2 K in the moderate field of 50 kG approaches the zero-field room-temperature value.

IV. DISCUSSION

The in-plane resistivities of RSb_2 ($R = \text{La-Nd, Sm}$) show metallic behavior ($d\rho/dT > 0$) with RRR ranging from about 40 to more than 400. Magnetic ordering reveals itself both in the loss of spin-disorder scattering in resistivity, and in anomalies in the magnetic susceptibility. Magnetic susceptibility for RSb_2 with $R = \text{Ce-Nd}$ also clearly shows local momentlike behavior at high temperatures. The values of the effective magnetic moment obtained from the susceptibility in the paramagnetic state are close to the theoretical values $g\sqrt{J(J+1)}$. The Curie-Weiss temperature Θ_p changes monotonically from CeSb_2 to NdSb_2 . For $H \parallel c$, Θ_p^c is negative for all three compounds [Fig. 25(a)] indicating that dominant interactions along the c axis are antiferromagnetic. Magnetic properties of RSb_2 with $R = \text{Ce-Nd, Sm}$ are anisotropic, probably due to the crystalline field effects. The c -axis anisotropy in the paramagnetic state decreases from



(a)



(b)

FIG. 23. (a) High-field temperature-dependent transverse magnetoresistance of NdSb_2 ; $I \parallel (ab)$, $H \parallel c$. (b) Field-dependent transverse magnetoresistance of NdSb_2 ; $I \parallel (ab)$, $H \parallel c$. Insets: high-field part of the $R(H)$ curve at $T = 2$ K, background subtracted; spectrum of Shubnikov-de Haas oscillations in NdSb_2 at 2 K.

$R = \text{Ce}$ to $R = \text{Nd}$ and further to $R = \text{Sm}$, where the difference between in-plane and normal to the plane susceptibilities is small and the sign of the anisotropy changes with temperature. It should be noted though, that since the light rare-earth diantimonides have orthorhombic symmetry, detailed analysis of the anisotropy can only be performed if the magnetization data along the high symmetry in-plane axes are known. The variation of the magnetic ordering temperatures of the magnetic rare-earth diantimonides from $R = \text{Ce}$ to $R = \text{Sm}$ is shown in Fig. 25(b) plotted as a function of the de Gennes factor, $DG = (g_J - 1)^2 J(J+1)$.

The magnetic interaction between the localized rare-earth magnetic moments in metallic RSb_2 ($R = \text{Ce-Nd, Sm}$) is probably due to the indirect exchange via conduction electrons of the Ruderman-Kittel-Kasuya-Yosida (RKKY) type. In this case the magnetic ordering temperature T_m may be approximated²⁰ by

$$T_m \propto 8N(E_F)/k_B I^2 (g_J - 1)^2 J(J+1) = 8N(E_F)/k_B I^2 DG,$$

where $N(E_F)$ is the conduction-electron density of states at the Fermi level, k_B is the Boltzmann constant, I is the exchange interaction parameter, g_J is the Lande g factor, J is the total angular momentum of the R ion, and

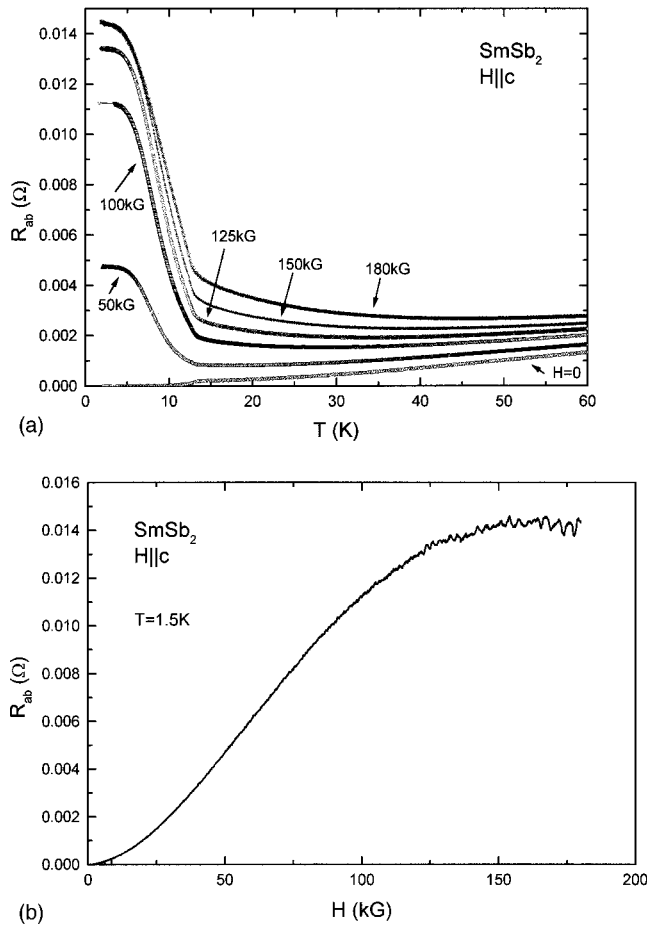


FIG. 24. (a) High-field temperature-dependent transverse magnetoresistance of SmSb_2 ; $I||ab$, $H||c$. (b) Field-dependent transverse magnetoresistance of SmSb_2 at $T=1.5$ K; $I||ab$, $H||c$.

$DG=(g_J-1)^2J(J+1)$ is the de Gennes factor. Experimentally, [Fig. 25(b)] T_m is not scaling with the de Gennes factor. Several reasons may be responsible for the deviation from the de Gennes scaling: crystalline field effects; variation of the exchange interaction constant I with the change of the lattice parameters through the series¹ due to the lanthanide contraction; change of the density of states within the series. It should be noted that the examination of the structural arrangements and the bond characters in AB_2 compounds (A -rare earth, $B=\text{Se, Te, Sb}$),¹ as well as the pressure dependence of resistance of PrSb_2 Ref. 6 strongly suggest that the conduction-electron density of states in the diantimonides depends significantly on the interatomic distances (i.e., lattice parameters). It is worth mentioning that in the mean-field approximation for the materials with RKKY interactions both the paramagnetic Curie-Weiss temperature and the magnetic ordering temperature have the same functional dependence on $N(E_F)$, I and DG . Comparing Fig. 25(a) with Fig. 25(b) we notice that while Θ_p of CeSb_2 is following the common trend for the other RSb_2 compounds, its T_m is way off the monotonic behavior. It can be hypothesized that at low temperatures the Ce ion in CeSb_2 has an intermediate, noninteger, valence between $3+$ and $4+$ that results in the addition of some electrons to the conduction band and change of $N(E_F)$ and I , while at high temperatures it behaves as Ce^{3+} . Detailed band-structure calculations

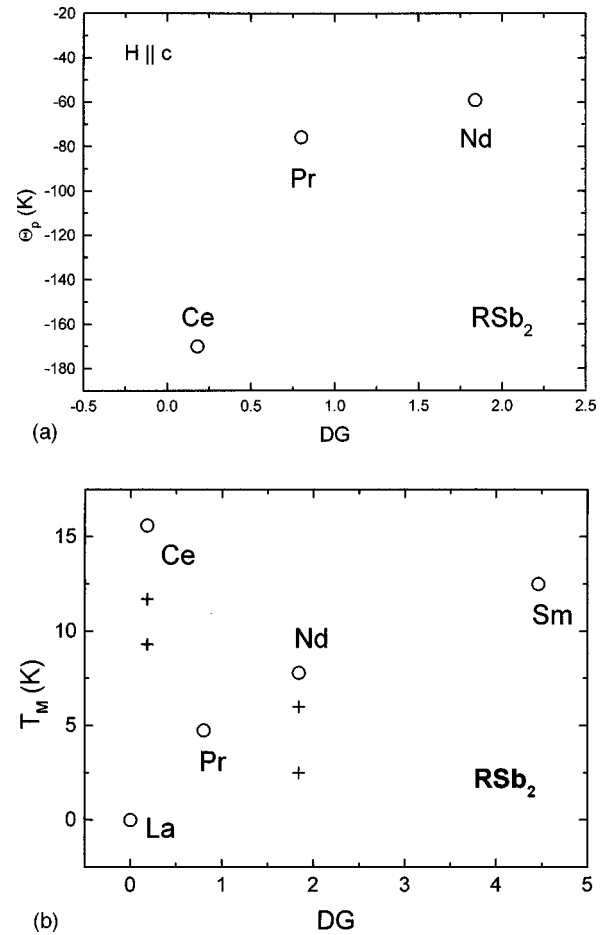


FIG. 25. (a) Paramagnetic Curie-Weiss temperatures; (b) magnetic ordering temperatures for RSb_2 as a function of $DG=(g_J-1)^2J(J+1)$, de Gennes factor. Note the highest ordering temperature is shown as an open circle with lower ordering temperatures (Ce and Nd) shown as crosses.

combined with carrier density measurements and determination of the crystalline electric-field parameters and spin arrangements at different temperatures (from neutron diffraction) are necessary to advance towards the full understanding of the magnetic properties of the series.

Metamagnetic transitions manifest themselves as sharp changes both in field-dependent magnetization, and in magnetoresistance. While these changes occur at the same fields, the relative values of jumps $\Delta\rho$ and ΔM do not necessarily correspond to each other. Several theoretical attempts have been undertaken to explain the temperature and field dependencies of resistivity in a local-moment magnetically ordered state. Miwa¹³ and Elliott and Wedgwood²¹ addressed the problem of the appearance of gaps in the conduction band due to antiferromagnetic order, in particular, in the case of screw-type spin arrangement developing the ideas of Slater²² and Mackintosh,²³ but these authors start with the assumption that the Fermi surface of the magnetic material in their calculations was taken to be free-electron-like. Later, a series of papers by Yamada and Takada²⁴ addressed the behavior of the magnetoresistivity of a simple axial antiferromagnet below and above the magnetic ordering transition as well as in the saturated paramagnetic state. The model of Yamada

and Takada²⁴ predicts a positive magnetoresistance $\Delta\rho(H)/\rho(0)\propto H^2$ in the antiferromagnetic state with the field along the direction of the spins and field-independent magnetoresistance for a magnetic field perpendicular to the spin direction. In contrast, in the saturated paramagnetic state the magnetoresistance is predicted to be negative with a field dependence $\Delta\rho(H,T)/\rho(0,T)\propto -(H-H_{c2})/T \exp(-\mu(H-H_{c2})/T)$, where H_{c2} is the critical magnetic field of the transition to saturated paramagnetic state and μ is the localized magnetic moment. For the diantimonides under study the magnetoresistance in the antiferromagnetic phase is positive, however it does not follow a simple H^2 law. Our measurements show a decrease of the magnetoresistance as the field-induced transition to the paramagnetic state occurs, albeit the functional dependence suggested in Ref. 24 for this case does not give reasonable fits to our data. The model of Yamada and Takada was developed only for a limited number of specific spin configurations, and does not describe the intermediate ordered phases formed as a result of metamagnetic transitions. This model cannot account for another significant experimental feature: an abrupt change of resistivity at the critical field of the metamagnetic transition.

In the model based on the picture of the energy gap formation, the temperature dependence of the resistivity in the local-moment antiferromagnetic state can be written¹³ as $\rho=(\rho_i+\rho_1(T)+\rho_m(T))/(1-gm(T))$, where ρ_i is resistivity due to impurity scattering (residual resistivity), ρ_1 is that due to lattice (electron-phonon) scattering, ρ_m is the magnetic component of resistivity, $m(T)$ is the normalized sublattice magnetization, and g is the parameter characterizing the effective change in the number of carriers due to the band-structure gapping. Both steplike changes in magnetization and possible changes of the effective number of carriers may be responsible for sharp changes of resistivity at the critical fields of metamagnetic transitions.

The high-temperature decrease of the absolute value of the negative in-plane magnetoresistance in CeSb₂ (Fig. 8) agrees with the behavior anticipated for Kondo lattices and Kondo-impurity systems.^{10,11} However, the same functional form $\Delta\rho(H)\propto H^2$ for the field-dependent negative magnetoresistance due to spin fluctuations in ferromagnetic materials was obtained in Ref. 24:

$$\rho(T,H)-\rho(T,0)\propto -|\ln(T-T_C)|H^2/(T-T_C)^2 - H^2/(T-T_C)^2$$

for different temperature limits above the Curie temperature T_C . Our $\rho(T,H)$ data for CeSb₂ for $H\parallel c$ can be fitted reasonably well with these functions. So, from the magnetization and magnetoresistance data alone the classification of CeSb₂ as a heavy fermion system with a magnetic ground state cannot be suggested unambiguously. The evaluation of the linear (in temperature) coefficient of the specific heat γ at low temperature in this system for $T<T_N$ as well as $T>T_N$ should help to resolve this ambiguity.

Despite the variation of the physical properties of RSb₂ ($R=\text{La, Pr-Sm}$), their magnetoresistance for $I\parallel(ab)$ in the paramagnetic state is quite similar (see Table I). As an example, s at 20 K is between 3.2 and 3.6 10^{-2} kG⁻¹ for $R=\text{Pr-Sm}$ and slightly higher (5.9) for $R=\text{La}$, although the variation in resistivity at 20 K is 7–8 times and the RRR

varies almost by an order of magnitude. Similarities are also observed in the temperature-dependent magnetoresistance curves measured at 55 kG [Figs. 3(a), 12, 17, and 21(a)]. For the transverse magnetoresistance with $H\parallel c$ the effect of field is higher and does not involve additional complications due to metamagnetism in this field range. A steep increase of $\rho(T,55\text{ kG})-\rho(T,0)$ is observed for the temperatures below the zero-field value of the magnetic ordering temperature, and the magnetoresistance in the ordered state is significantly higher than in the paramagnetic state. In the paramagnetic state the magnetoresistance of all members except CeSb₂ increases rapidly as the temperature is lowered even for LaSb₂, for which no magnetic transition was observed down to the lowest temperature investigated. Qualitatively similar behavior of the temperature-dependent magnetoresistance with $I\parallel c$ was observed in LaSb₂ and SmSb₂.

The magnetoresistance of the diantimonides at low temperatures is notably high. In a simple, free-electron-like approach²⁵ the condition $\omega_c\tau\gg 1$, where ω_c is cyclotron frequency and τ is relaxation time, is required for complete cyclotron orbits. This inequality can be written as $\omega_c\tau=H/ne\rho_0\gg 1$, where H is the applied magnetic field, n is the density of carriers, e is the charge of electron, and ρ_0 is the resistivity. At low temperatures the diantimonides have low resistivity ($\rho_0\approx 10^{-6}$ Ω cm). Moreover, according to the analysis of the structure and band character in AB_2 compounds,¹ while $R\text{Se}_2$ and $R\text{Te}_2$ are still semiconductors, RSb_2 are just entering into the metallic category, so low carrier density is expected for the diantimonides. Both these factors are favorable for high magnetoresistance at low temperatures. The anisotropy of the magnetoresistance might reflect the anisotropy of the Fermi surface and/or electron-phonon and electron-electron interactions.

The theory of the galvanomagnetic properties of a normal metal with an arbitrary energy spectrum was developed by Lifshits and co-workers²⁶ and verified for most of the simple metals.²⁷ For transverse magnetoresistance in the high-field limit, the theory predicts either saturation or $\Delta\rho(H)\propto H^2$, depending upon the topology of the Fermi surface. On the other hand, the asymptotic behavior of the longitudinal magnetoresistance is independent of the topology of the Fermi surface and $\Delta\rho(H)$ is expected to saturate in high fields. Our experimental data for the diantimonides for both transverse and longitudinal magnetoresistance differ from these simple theoretical predictions of Ref. 26. Deviations from the theory of Lifshits and co-workers were observed earlier in a number of cases, in particular, high, linear, magnetoresistance was observed in quasi-2D materials: NbSe₂ [$s(8\text{ K})\approx 1.1\times 10^{-2}$ kG⁻¹];²⁸ some of the $2H\text{-}MX_2$ polytypes of transition metal dichalcogenides for $H\geq 10\text{--}20$ kG: $2H\text{-NbSe}_2$ [$s(4.2\text{ K})\approx 2.3\times 10^{-2}$ kG⁻¹], $2H\text{-TaSe}_2$ [$s(4.2\text{ K})\approx 5.2\times 10^{-2}$ kG⁻¹];²⁹ as well as in isotropic (bcc) single crystals of potassium [$s(4.2\text{ K})\approx 0.9\times 10^{-2}$ kG⁻¹] Ref. 30 and a few other metals.

Several theories resulting in linear magnetoresistance were suggested. Critical analysis of some of them was given in Refs. 25 and 31. A few of these theories^{31–34} require *special orientations* of the magnetic field with respect to the Fermi surface and/or *particular features* of the Fermi surface or the ground state defined by spin-or charge-density wave. In RSb₂ ($R=\text{La, Pr, Nd}$) near-linear magnetoresistance was

observed both for unique, normal to (*ab*) plane, and arbitrary, in-plane, field directions up to $H_{\max}=55$ kG (experimental field limit). In LaSb₂ linear magnetoresistance was observed also for $I\parallel c$. In PrSb₂ no significant changes in magnetoresistance were associated with the charge-/spin-density wavelike anomaly [Fig. 10(b)]. So none of the above mechanisms appear to fully account for the large linear magnetoresistance in RSb₂ ($R=\text{La, Pr, Nd}$), though some of them may contribute to the observed behavior.

Several other more general “intrinsic transport theories” that do not suffer some of the limitations of the ones mentioned above, have been proposed. One of them, the so-called “hot-spot” model,³⁵ requires strong scattering probabilities between small well-defined spots on opposite sides of the Fermi surface and predicts linear magnetoresistance for $\omega_c\tau\gg 1$, $\omega_cT\ll 1$. Another one³⁶ considers many-body effects and in calculating the relaxation time shows that the magnetic field introduces symmetry breaking in a scattering process, which substantially increases the linear contribution to the magnetoresistance so that this contribution may become dominant. This mechanism was used to explain linear, positive, magnetoresistance of heavy fermion CeCu₆ at very low temperatures.¹² Yet another model³¹ is based on the existence of fluctuations into a quasiperiodic static state that has the anisotropy of the lattice and may be due to electron-phonon and electron-electron interactions (i.e., fluctuations into a spin-density or charge-density-wave state). This mechanism contributes equally to a linear increase in longitudinal and transverse magnetoresistance. The validity of the first two models for normal metals was questioned (respectively, in Refs. 31 and 25). The last one seems to be attractive since it accounts for the similar values of in-plane transverse and longitudinal magnetoresistance observed throughout the whole series and the anisotropy between the $H\parallel(ab)$ and $H\parallel c$ cases.

Another theoretical model was used to explain peculiar magnetotransport properties of quasi-two-dimensional single-crystal graphite at low temperatures.³⁷ For the magnetic field applied perpendicular to the (*ab*) plane two phenomena resembling the behavior of the light rare-earth dantimonides were observed: in high magnetic fields the experimentally observed magnetoresistance of graphite can be represented by $\rho(H)=H/(p+qH^n)$, $n\approx 1$; and in strong fields the resistivity $\rho(H,T)$ as a function of temperature goes through a broad maximum (at 20–30 K), dependent of field.³⁷ The model of magnetic freeze-out of the impurity carriers was invoked to explain the observed behavior. It was assumed that the processes $D^+ + (-e)\rightarrow D^0$ and/or $A^- + (+e)\rightarrow A^0$, where D^+ corresponds to donor, A^- represents acceptor, $(-e)$ is the electron and $(+e)$ is the hole, are induced in strong magnetic field. Then coexistence of the ionized impurity scattering and the neutral impurity scattering at low temperatures together with the contribution from the electron-phonon and carrier-carrier scattering at higher temperatures can give the physical picture qualitatively consistent with the experimental data. It is worth mentioning that LaSb₂ and PrSb₂ have the lowest RRR, i.e., the highest impurity scattering within the series, and the effect of magnetic field on the resistivity in the paramagnetic state is more pronounced. This seems to be consistent with the freeze-out model, where the impurity scattering plays an important role.

However, several problems have to be mentioned regarding the general use of the freeze-out model for the light rare-earth dantimonides: although this model was applied to graphite it was initially formulated for semiconductors and the extension of this model to semimetals is not obvious; the dantimonides have large residual resistance ratios, very small residual resistivity and large magnetoresistance at low temperatures. With this in mind, the assumption that such a significant contribution originates from changes of the impurity scattering seems doubtful. Finally, the magnetic freeze-out model is sensitive to the details of the band structure of the material, and the measurements of the magnetoresistance ($H\parallel c$) for PrSb₂ under pressure⁶ show large (~5 times) decrease of the zero-field resistance at 2 K under pressure up to 11.5 kbar, pointing to the possible changes of the band structure and/or concentration or mobility of carriers. However, the absolute change of resistivity in the field up to 50 kG [$\rho(2\text{ K}, 50\text{ kG})-\rho(2\text{ K}, 0)$] in this pressure range is practically constant, and this behavior cannot be easily understood by the simple extension of the freeze-out model. Detailed studies in higher magnetic fields and employment of other experimental techniques (Hall effect, etc.) are required to test the applicability of theoretical models of the linear magnetoresistance for RSb₂.

Another issue that needs more detailed examination is the steep increase of the magnetoresistance (for $H\parallel c$) in RSb₂ ($R=\text{Pr, Nd, Sm}$) at temperatures lower than the zero-field magnetic ordering transition temperature. For the field along the *c*-axis the position of the “break” in the low-temperature resistivity is not shifting significantly in the applied field up to 180 kG [Figs. 23(a), and 24(a)] so, for this orientation, the Néel temperature is not changing over a large magnetic-field range. To address the issue we can attempt to invoke a general, rather than specific, view on transport properties of metals. Within the framework of Matthiessen’s rule, we can consider separately different scattering mechanisms at low temperatures: electron-impurity, electron-phonon, and electron-localized spins. The values of RRR are very high in the dantimonides, and we do not expect the electron-impurity scattering to change drastically through the magnetic transition; electron-phonon scattering is not expected to be dominant at the 2–10 K temperature range, so it is doubtful that these two mechanisms are responsible for the steep increase of the magnetoresistance. However, since the sharp “break” in the magnetoresistance occurs close to the Néel temperature, it is tempting to attribute it to the changes in the electron-localized spin scattering. Below the magnetic ordering temperature the relaxation time τ increases due to a loss of spin-disorder scattering, bringing the sample further towards the condition $\omega_c\tau\gg 1$ needed for large magnetoresistance.

In order to further investigate the importance of relaxation time, another general rule can be used to examine the magnetoresistance both in the ordered and in the paramagnetic state. In many metals and semimetals the behavior of magnetoresistance is known to follow Kohler’s rule.³⁸ The Kohler’s rule is a similarity law for magnetoresistance. It is based on the idea of the universal mean-free path that does not depend on the electron momentum. It is usually written as $\Delta\rho/\rho_0=F(H/\rho_0)$ where $\Delta\rho=\rho(T,H)-\rho(T,0)$ and $\rho_0=\rho(T,0)$. In the analysis of the magnetoresistance of

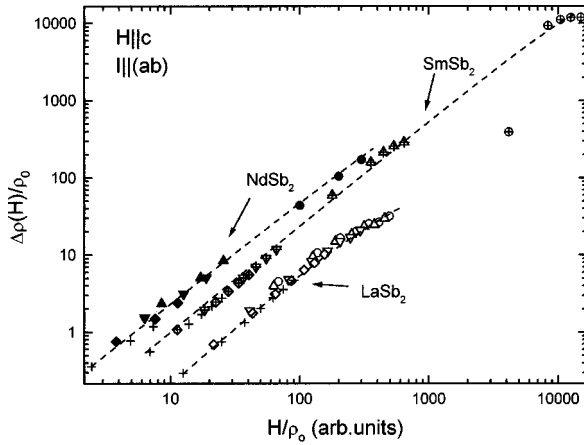


FIG. 26. “Kohler”-like plot of the transverse magnetoresistance of RSb_2 ($R=La, Nd, Sm$). Data from the high-field measurements [Figs. 22, 23(a), and 24(a)]. Symbols: circles: $T=2$ K, up triangles: $T=10$ K, down triangles: $T=20$ K, diamonds: $T=30$ K, crosses: $T=40$ K. Lines are guides for the eye.

graphite³⁹ Kohler’s rule was used in a more general form, presumably derived from the two-band model: $\Delta\rho/\rho_0 = F(\mu H)$ where μ is the geometric mean of the electron and hole mobilities and may be temperature dependent. For the light rare-earth dantimonides in the case of the applied field parallel to the c -axis, where no metamagnetic transitions are observed in $\rho(H)$ isotherms, Kohler’s rule is approximately valid in a large temperature range ($T \leq 50$ K) (Fig. 26), both below and above the magnetic ordering transitions. The $\ln(\Delta\rho(H)/\rho_0)$ data are approximately falling onto the universal (for each material) lines vs $\ln(H/\rho_0)$ with the slope around 1–1.3. In a more detailed analysis, since the magnetoresistance is approximately following the same power law as a function of field, the “generalized” Kohler’s rule is probably more appropriate in the whole temperature range.

One more result that requires more investigation is the saturation of the transverse magnetoresistance [$H||c, I||(ab)$] in $SmSb_2$ in the fields $H \approx 150$ kG [Fig. 24(b)], well above the $\omega\tau > 1$ limit when de Haas-van Alphen oscillations first occur (≈ 15 kG at 2 K). While a knowledge of the Fermi surface is necessary to analyze this change of $\rho(H)$ behavior, there is a possibility that we observe the phenomenon similar to the one studied in Zn, where as it is in our case, the $\rho(H)$ behavior changes to saturation in high fields where Shubnikov-de Haas oscillations start to appear.⁴⁰ This phenomenon was explained by assuming that at some field a

magnetic breakdown starts to take place, the resulting new closed electron orbits include different parts of the Fermi surface and the low-field compensation of the carriers [that gives infinite increase of $\rho(H)$ with field] is broken, with the consequence that transverse magnetoresistance saturates (as expected for high-field behavior of noncompensated metals with closed orbits).²⁶

V. CONCLUSIONS

We have studied the evolution of magnetic and magnetotransport properties of single crystals of quasi-2D RSb_2 ($R=La-Nd, Sm$) compounds. All except $LaSb_2$ have magnetically ordered ground states with a complex sequence of several ordered phases at $H=0$ for $CeSb_2$ and $NdSb_2$. Three of the members of the series ($R=Ce, Pr, Nd$) exhibit metamagnetic transitions, as observed by $M(H)$ and $\rho(H)$ measurements at low temperatures. Temperature-dependent magnetization of the magnetic dantimonides is highly anisotropic (due to crystalline field effect splitting) with the c axis being a hard magnetization axis. Metamagnetic transitions observed for some of the members of the series show in-plane anisotropy. The magnetoresistance of the dantimonides in the paramagnetic state is anisotropic and close to linear for $R=La, Pr, Nd$. The relative change of resistivity in magnetic field is remarkably high.

The complexity and diversity of the physical properties of the light rare-earth dantimonides makes the series interesting for future studies. A few points that are particularly worth addressing are spin structure of the different magnetically ordered phases occurring both in zero field and as a result of metamagnetic transitions; extension of the $\rho(H)$ measurements to substantially higher fields; study (both experimental and theoretical) of the band structure of the dantimonides and its changes with the rare earth.

ACKNOWLEDGMENTS

We thank I. R. Fisher for the critical reading of the manuscript and fruitful discussions. Ames Laboratory is operated for the U.S. Department of Energy by Iowa State University under Contract No. W-7405-Eng-82. This work was supported by the Director for Energy Research, Office of Basic Energy Sciences. Work at NHMFL-Los Alamos Facility was performed under the auspices of the National Science Foundation and the Department of Energy. One of us (S.L.B.) was partially supported by IITAP-Iowa State University and CNPq (Brazil) in the final stage of the work.

¹R. Wang and H. Steinfink, *Inorg. Chem.* **6**, 1685 (1967).

²F. Hullinger, in *Handbook of Physics and Chemistry of Rare Earths*, edited by K. A. Gschneidner and L. Eyring (North-Holland, Amsterdam, 1979), Vol. 4, p. 153.

³F. Hullinger and H. R. Ott, *J. Less-Common Met.* **55**, 103 (1977).

⁴P. C. Canfield, J. D. Thompson, and Z. Fisk, *J. Appl. Phys.* **70**, 5992 (1991).

⁵E. Bucher (private communication).

⁶G. Oomi, T. Kagayama, K. Kawaguchi, P. C. Canfield, and S. L. Bud’ko, *Physica B* **230–232**, 776 (1997).

⁷K. Kawaguchi, T. Kagayama, G. Oomi, P. C. Canfield, and S. L. Bud’ko, *Physica B* **237–238**, 587 (1997).

⁸P. C. Canfield and Z. Fisk, *Philos. Mag. B* **65**, 1117 (1992).

⁹*Binary Alloy Phase Diagrams*, edited by T. B. Massalski, H. Okamoto, P. R. Subramanian, and L. Kacprzak (ASM International, Materials Park, OH, 1992).

¹⁰See, for example, P. Schlottmann, *Phys. Rep.* **181**, 1 (1989).

¹¹N. Kawakami and A. Okiji, *J. Phys. Soc. Jpn.* **55**, 2114 (1986).

¹²P. T. Coleridge, *J. Phys. F* **17**, L79 (1987).

¹³H. Miwa, *Prog. Theor. Phys.* **29**, 477 (1963).

- ¹⁴E. Fawcett, H. L. Alberts, Yu. Galkin, D. R. Noakes, and J. V. Yakhmi, *Rev. Mod. Phys.* **66**, 25 (1994).
- ¹⁵See, for example, J. M. Lawrence, P. S. Riseborough, and R. D. Parks, *Rep. Prog. Phys.* **44**, 1 (1981).
- ¹⁶See, for example, *Electrons at the Fermi Surface*, edited by M. Springford (Cambridge University Press, Cambridge, England, 1980), and references therein.
- ¹⁷I. M. Lifshits and A. M. Kosevich, *Zh. Eksp. Teor. Fiz.* **29**, 730 (1955) [*Sov. Phys. JETP* **2**, 636 (1956)].
- ¹⁸C. H. Mielke, N. Harrison, A. Lacerda, S. L. Bud'ko, and P. C. Canfield (unpublished).
- ¹⁹P. M. Chaikin, *Phys. Rev. B* **31**, 4770 (1985).
- ²⁰M. B. Maple, in *Ternary Superconductors*, edited by G. K. Shenoy, B. D. Dunlap, and F. Y. Fradin (North-Holland, Amsterdam, 1981), p. 131.
- ²¹R. J. Elliott and F. A. Wegdwood, *Proc. Phys. Soc. London* **81**, 846 (1963).
- ²²J. C. Slater, *Phys. Rev.* **82**, 538 (1951).
- ²³A. R. Mackintosh, *Phys. Rev. Lett.* **9**, 90 (1962).
- ²⁴H. Yamada and S. Takada, *Prog. Theor. Phys.* **48**, 1828 (1972); *ibid.* **49**, 1401 (1973); *J. Phys. Soc. Jpn.* **34**, 51 (1973).
- ²⁵A. B. Pippard, *Magnetoresistance in Metals* (Cambridge University Press, Cambridge, England, 1989).
- ²⁶For a review see, I. M. Lifshits, M. Ya. Azbel, and M. I. Kaganov, *Electron Theory of Metals* (Consultant Bureau, New York, 1973).
- ²⁷For a review see, E. Fawcett, *Adv. Phys.* **13**, 139 (1964).
- ²⁸F. Roeske, Jr., H. R. Shanks, and D. K. Finnemore, *Phys. Rev. B* **16**, 3929 (1977).
- ²⁹M. Naito, S. Tanaka, and N. Miura, in *Physics in High Magnetic Field*, edited by S. Chikazumi and M. Miura (Springer, New York, 1981), p. 320.
- ³⁰P. A. Penz and R. Bowers, *Phys. Rev.* **172**, 991 (1968).
- ³¹L. M. Falicov and H. Smith, *Phys. Rev. Lett.* **29**, 124 (1972).
- ³²L. M. Falicov and P. R. Sievert, *Phys. Rev.* **138**, A88 (1965).
- ³³L. M. Falicov and M. J. Zuckermann, *Phys. Rev.* **160**, 372 (1967).
- ³⁴A. G. Lebed and N. N. Bagmet (unpublished).
- ³⁵R. A. Young, *Phys. Rev.* **175**, 813 (1968).
- ³⁶G. D. Mahan, *J. Phys. F* **13**, L257 (1983).
- ³⁷K. Sugihara and J. A. Woolam, *J. Phys. Soc. Jpn.* **45**, 1891 (1978), and references therein.
- ³⁸See, for example, A. A. Abrikosov, *Fundamentals of the Theory of Metals* (North-Holland, Amsterdam, 1988).
- ³⁹K. Noto and T. Tsuzuki, *Carbon* **12**, 209 (1974).
- ⁴⁰See, for example, A. B. Pippard, in *The Physics of Metals I. Electrons*, edited by J. M. Ziman (Cambridge University Press, Cambridge, England, 1969), p. 113 and references therein.